Three-Frequency Nonlinear Heterodyne Detection. 1: cw Radar and Analog Communications

Malvin Carl Teich and Rainfield Y. Yen

Though heterodyne detection provides a valuable technique for detecting small signals, the conventional system has several inherent disadvantages. In applications such as communications and radar, obtaining a reasonably high signal-to-noise ratio (SNR) requires (1) a good knowledge of the velocity of the transmitter or target, (2) a stable yet tunable local oscillator, and (3) a target or source that presents a minimum of frequency broadening. These conditions are frequently not adhered to by real systems, particularly in the ir and optical, giving rise to detection capabilities far below optimum. Calculations are presented for the use and operation of a three-frequency nonlinear heterodyne system that eliminates many of the stringent conditions required for conventional heterodyne detection, while maintaining its near-ideal SNR. The technique, which is similar in principle to heterodyne radiometry, makes use of a two-frequency transmitter and a nonlinear second detector and is particularly useful for signal acquisition; for signals of unknown Doppler shift, in fact, performance is generally superior to that of the conventional system. Although primary emphasis is on the ir and optical because of the large Doppler shifts encountered there, application of the principle in the microwave and radiowave is also discussed. For cw radar and analog communications, the SNR, power spectral density (PSD), and minimum detectable power (MDP) are obtained and compared with the standard configuration. Both sinewave and Gaussian input signals are treated. A variety of specific cases are discussed including the optimum performance case, the typical radar case, and the AM and FM communications case. Evaluation of the technique for pulsed radar and digital communications applications (both in the absence and in the presence of the lognormal atmospheric channel) is reserved for Part 2 of this paper [Appl. Opt. 14, 680 (1975)].

I. Introduction

Heterodyne detection is useful in several configurations, among which are the detection of scattered or reflected radiation from a moving target (Doppler radar) and communications.[1] Its use has been demonstrated in many regions of the electromagnetic spectrum including the ir,[2–5] the visible,[6–11] and the microwave. Its advantages as a detection technique are well known: high sensitivity, frequency selectivity, and strong directivity. For radar applications, it provides a major method of recovering desired signals and removing clutter. The significant improvement in sensitivity that it provides arises from knowledge of the Doppler frequency (also called the heterodyne frequency or the intermediate frequency, IF), which permits a narrow receiver bandwidth centered about the IF. If, in the case of a radar or a space communications link, the received signal is very strong or the radial target (transmitter) velocity is known, this is easily accomplished. In an earth-based communication system, the same applies provided the frequency difference between the transmitter and local oscillator (LO) is known.

The extension of microwave heterodyne techniques into the ir and visible, and the attendant increase in the Doppler shift by many orders of magnitude for target of a given velocity, has provided better target resolution capabilities;[10] but there have been attendant difficulties. If the radial velocity of a target or the frequency difference between the transmitter and LO in a communications system has not been established, for example, then the heterodyne frequency is not known, and it may be very difficult to acquire a weak signal using the standard technique. In fact, an unknown IF may necessitate the use of broad bandwidth detection and electronics, resulting in a degraded signal-to-noise ratio (SNR), or perhaps the use of frequency scanning of the receiver or the LO. The rate of such scanning is, of course, limited by the time response of the system. Furthermore, to keep the heterodyne signal within the electrical passband of the system, the LO frequency must

M. C. Teich is with the Department of Electrical Engineering & Computer Science, Columbia University, New York, New York 10027 and is a Fellow of the John Simon Guggenheim Memorial Foundation. R. Y. Yen was with Columbia University; he is now with Columbia Research Corporation, Gaithersburg, Maryland, 20760.

Received 17 May 1974.

be relatively stable with reference to the signal frequency and yet tunable so it can track the Doppler shift, which varies in time. Returns from nonsolid targets (e.g., gases and plasmas) are generally broader than returns from solid targets, due to the constituent particle velocity distribution—thus demanding larger bandwidths. It is noted that these various difficulties are more acute in the ir and optical, where large values of the IF are encountered (Doppler-shift is proportional to the radiation frequency).

In this paper we discuss the operation of a three-frequency nonlinear heterodyne detection scheme for cw radar and analog communications use. The concept, which is similar to heterodyne radiometry, was first proposed in 1969 by Teich,[1] and experimentally examined in 1972 by Abrams and White.[12] It provides the near-ideal SNR offered by conventional heterodyne detection, while eliminating many of the difficulties discussed above. In Part 2 of this paper[13] we apply the scheme to digital communications and pulsed radar.

As defined by our usage, the designation nonlinear refers to the electronics following the detector and not to the process itself, which could always be referred to as nonlinear since it involves mixing or multiplication. In this system, *two* signals of a small but well-known difference frequency, $\Delta\nu$, are transmitted. With the LO frequency, f_L, we have a three-frequency mixing system. Aside from the heterodyne mixer, a *nonlinear* element such as a square-law device is included to provide an output signal at a frequency very close to $\Delta\nu$ regardless of the Doppler shift of the transmitted signals. This scheme obviates the need for high-frequency electronics, thus improving impedance matching, system noise figure, and range of operation over the conventional case. The usual frequency scanning is eliminated as is the necessity for a stable LO. And, it allows targets to be continuously observed with Doppler shifts of considerably greater magnitude and range than previously possible. This is particularly important in the ir and optical, where Doppler shifts are generally large,[10] and the importance of this technique is expected to be emphasized in these regions. Furthermore, it is possible for the three-frequency system to have a higher output SNR than the conventional system, as we will show later. Problems in the tracking of nonsolid targets are minimized since Doppler information is eliminated; nevertheless, an additional tunable filter may be inserted in the system if Doppler information is required. We investigate the sine-wave signal case as well as the Gaussian signal case with both Gaussian and Lorentzian spectra. The main results are expressed as the output SNR for the system in terms of the input SNR.

II. Configuration

In Figure 1, we present a block diagram for a radar version of the system. A transmitter emits two waves of frequencies f_1 and f_2, whose difference $f_c = |f_1 - f_2| = \Delta\nu$ is known to high accuracy. (This is particularly easy to accomplish if the transmitter is a two-mode laser, since the modes tend to drift together keeping f_c constant, or if it is a single-frequency laser modulated into two frequency components.) The waves are Doppler shifted by the moving target, the nature of which is unimportant. Thus, a wave of frequency f will return with a frequency f' given by the standard nonrelativistic Doppler shift formula

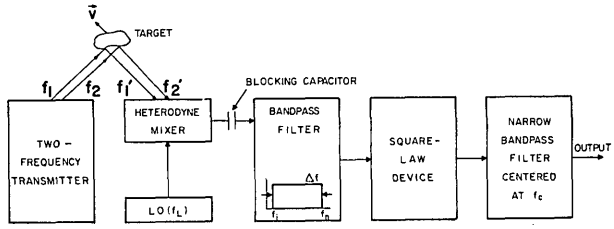

Fig. 1. Block diagram of the three-frequency nonlinear heterodyne system for radar application.

$$f' = f(1 \pm 2v_{\parallel}/c), \tag{1}$$

where $v_{\parallel}$ is the radial velocity of the target and c is the speed of light. Therefore, after scattering from the target, and choosing $f_1 > f_2$, the new frequency difference between the two waves f_c' is given by

$$f_c' = f_1' - f_2' = f_c \pm (2v_{\parallel}/c)f_c. \tag{2}$$

Aside from the frequency shift that results from the Doppler effect, there may be a frequency broadening of each wave associated with the scattering by a moving target in a typical radar configuration. For a rotating target, this broadening is of the order $4R\omega_{\perp}/\lambda$, where R is the radius of the target, $\omega_{\perp}$ is its component of angular velocity perpendicular to the beam direction, and λ is the wavelength of the transmitted signal.[4] For practical systems, as will be shown later, the difference $f_c' - f_c$ is much smaller than the broadening effects and may usually be neglected. We can therefore choose $f_c' = f_c$ with high accuracy.

The receiver includes a heterodyne mixer with an LO followed by a blocking capacitor and a bandpass filter with bandwidth $\Delta f = f_n - f_i$. Here f_n and f_i are the upper and lower cutoffs, respectively, of the bandpass filter. When Doppler information is poor (in which case the three-frequency system is particularly useful), Δf will be large so it will cover a wide frequency range. In the following, we therefore pay particular attention to the case where $f_i \to 0$, so $\Delta f = f_n$. The noise arising from the strong LO is assumed to be shot noise, which in the high current limit becomes Gaussian, as illustrated by Davenport and Root.[14] To good approximation, the spectrum may be taken to be white. The latter part of the receiver is a square-law (or other nonlinear) device and a narrow bandpass filter centered at frequency $f_c = |f_1 - f_2|$. The details of the system are given in the following sections.

III. Three-Frequency Heterodyne Mixer

The mixer consists of a photodetector and a local oscillator. We are interested in determining the signal-to-noise ratio at the output of the photodetector. The input electric field consists of three plane, parallel, and coincident electromagnetic waves that are assumed to be polarized and to impinge normally on the photodetector. Spatial first-order coherence is assumed over the detector aperture. The total incident electric field E_t may therefore be written as

$$E_t = A_1 \cos(\omega_1 t + \varphi_1) + A_2 \cos(\omega_2 t + \varphi_2) + A_L \cos(\omega_L t + \varphi_L). \quad (3)$$

Here ω_1 and ω_2 are the angular frequencies of the two incoming signals, φ_1 and φ_2 are their phases, and ω_L is the angular frequency of the LO beam. The quantities A_1, A_2, and A_L are the amplitudes of the three waves, all of which are assumed to have the same plane polarization. In the ir and optical, the output of a photodetector or mixer is proportional to the total intensity of the incoming waves. Taking into account the quantum electrodynamics of photon absorption by optical and ir detectors,[5,11,15,16] the output signal r consists only of difference-frequency terms and dc terms. Thus

$$r = \beta\{A_1^2 + A_2^2 + A_L^2 + 2A_1A_L \cos[(\omega_1 - \omega_L)t + (\varphi_1 - \varphi_L)] + 2A_2A_L \cos[(\omega_2 - \omega_L)t + (\varphi_2 - \varphi_L)] + 2A_1A_2 \cos[(\omega_1 - \omega_2)t + (\varphi_1 - \varphi_2)]\}, \quad (4)$$

where β is a proportionality constant containing the detector quantum efficiency. If the incident waves are not spatially first-order coherent and/or polarized in the same direction, the usual decrease in r will occur.[2,3,5–8]

Since the LO beam may be made much stronger than those of the two signals, i.e., $A_L \gg A_1, A_2$, we can write

$$r \cong \beta A_L^2\{1 + (2A_1/A_L) \cos[(\omega_1 - \omega_L)t + (\varphi_1 - \varphi_L)] + (2A_2/A_L) \cos[(\omega_2 - \omega_L)t + (\varphi_2 - \varphi_L)]\}. \quad (5)$$

The term containing $\omega_1 - \omega_2$ has been neglected because of its relatively small amplitude. We now define

$$r_{dc} \equiv \beta(A_1^2 + A_2^2 + A_L^2) \cong \beta A_L^2, \quad (6a)$$

and

$$r_{IF} \equiv 2\beta A_1A_L \cos[(\omega_1 - \omega_L)t + (\varphi_1 - \varphi_L)] + 2\beta A_2A_L \cos[(\omega_2 - \omega_L)t + (\varphi_2 - \varphi_L)] = r_{dc}\{(2A_1/A_L) \cos[(\omega_1 - \omega_L)t + (\varphi_1 - \varphi_L)] + (2A_2/A_L) \cos[(\omega_2 - \omega_L)t + (\varphi_2 - \varphi_L)]\}. \quad (6b)$$

The mean-square photodetector response is then given by

$$\langle r_{IF}^2 \rangle = [2A_1^2/A_L^2 + 2A_2^2/A_L^2]r_{dc}^2 = 2r_{dc}^2(P_1 + P_2)/P_L, \quad (7)$$

where P_1, P_2, and P_L are the radiation powers in the two signal beams and in the LO beam, respectively.

If we consider the noise response r_n of the detector as arising from shot noise, which is the case for the photoemitter and the ideal reverse-biased photodiode,[3,5,11] the mean-square noise response is given by the well-known shot-noise formula[3,17]

$$\langle r_n^2 \rangle = 2er_{dc}\Delta f, \quad (8)$$

in which Δf is the noise response bandwidth and is determined by the Doppler uncertainty, and e is the electronic charge. For a comparatively strong LO, we have

$$r_{dc} = \eta eP_L/hf_L, \quad (9)$$

where η is the quantum efficiency and h is Planck's constant.

From Eqs. (7), (8), and (9), the signal-to-noise power ratio $(SNR)_{power}$ is given by

$$(SNR)_{power} = \langle r_{IF}^2 \rangle / \langle r_n^2 \rangle = \eta(P_1 + P_2)/hf_L\Delta f, \quad (10a)$$

which is seen to be independent of P_L. If we define $P_r \equiv P_1 + P_2$, and let $\nu = f_L \approx f_1 \approx f_2$, and $(SNR)_i = (SNR)_{power}$, we obtain

$$(SNR)_i = \eta P_r/h\nu\Delta f. \quad (10b)$$

Now P_r is the total input signal power, and $(SNR)_i$ is referred to as the input signal-to-noise ratio to the square-law device following the photodetector.

IV. Full-Wave Square-Law Device

By use of a blocking capacitor, the dc part of the photodetector response r_{dc} can be filtered out. The signal, which then has zero mean, is sent to a full-wave square-law device. If we let

$$s_a(t) = 2\beta A_1A_L \cos[(\omega_1 - \omega_L)t + (\varphi_1 - \varphi_L)]$$

and

$$s_b(t) = 2\beta A_2A_L \cos[(\omega_2 - \omega_L)t + (\varphi_2 - \varphi_L)],$$

and let $n(t)$ be the noise, then using a generalization of the direct method of Davenport and Root,[18] we can write the input to the square-law device $x(t)$ as

$$x(t) = s_a(t) + s_b(t) + n(t). \quad (11)$$

The output of the square-law device $y(t)$ is then given by

$$y(t) = \alpha x^2(t) = \alpha[s_a^2(t) + s_b^2(t) + n^2(t) + 2s_a(t)s_b(t) + 2s_a(t)n(t) + 2s_b(t)n(t)], \quad (12)$$

where α is a scaling constant. For a stationary random process, the expectation value of $y(t)$ is

$$E[y] = \alpha(E[s_a^2] + E[s_b^2] + E[n^2]) = \alpha(\sigma_a^2 + \sigma_b^2 + \sigma_n^2) \quad (13)$$

for all t, where E denotes the expectation value. In Eq. (13), we have set $\sigma_a^2 = E[s_a^2]$, $\sigma_b^2 = E[s_b^2]$, and $\sigma_n^2 = E[n^2]$. Furthermore,

$$y^2(t) = \alpha^2[s_a(t) + s_b(t) + n(t)]^4, \quad (14)$$

from which the mean-square value of $y(t)$ is evaluated to be

$$E[y^2] = \alpha^2(E[s_a^4] + E[s_b^4] + E[n^4] + 6\sigma_a^2\sigma_b^2 + 6\sigma_a^2\sigma_n^2 + 6\sigma_b^2\sigma_n^2). \quad (15)$$

In obtaining Eqs. (13) and (15), we have assumed that $s_a(t)$, $s_b(t)$, and $n(t)$ are all independent of each another, and that $E[s_a] = E[s_b] = E[n] = 0$.

The autocorrelation function of the output of the square-law device is

$$R_y(t_1, t_2) = E[y_1 y_2] = \alpha^2 E[(s_{a1} + s_{b1} + n_1)^2(s_{a2} + s_{b2} + n_2)^2]. \quad (16)$$

For stationary processes, setting $\tau = t_1 - t_2$, we obtain

$$R_y(\tau) = R_{a\times a}(\tau) + R_{b\times b}(\tau) + R_{n\times n}(\tau) + R_{a\times b}(\tau) + R_{a\times n}(\tau) + R_{b\times n}(\tau), \quad (17)$$

in which

$$R_{a\times a}(\tau) = \alpha^2 R_{a^2}(\tau), \quad (18a)$$

$$R_{b\times b}(\tau) = \alpha^2 R_{b^2}(\tau), \quad (18b)$$

$$R_{n\times n}(\tau) = \alpha^2 R_{n^2}(\tau), \quad (18c)$$

$$R_{a\times b}(\tau) = 4\alpha^2 R_a(\tau)R_b(\tau) + 2\alpha^2\sigma_a^2\sigma_b^2, \quad (18d)$$

$$R_{a\times n}(\tau) = 4\alpha^2 R_a(\tau)R_n(\tau) + 2\alpha^2\sigma_a^2\sigma_n^2, \quad (18e)$$

$$R_{b\times n}(\tau) = 4\alpha^2 R_b(\tau)R_n(\tau) + 2\alpha^2\sigma_b^2\sigma_n^2, \quad (18f)$$

with

$$R_{a^2}(\tau) = E[s_{a1}^2 s_{a2}^2], \quad R_a(\tau) = E[s_{a1}s_{a2}], \text{ etc.}$$

If we know the exact forms of these correlation functions, we can use the Fourier transform to obtain the power spectral density of the output that will, in turn, enable us to evaluate the final output signal-to-noise power ratio for the three-frequency system.

V. Pure Sinewave Input Signals

A. Input Power Spectral Density

We now assume that the two inputs to the photodetector are pure sinusoidal waves with constant phase over the spatial extent of the photodetector. This would be the case, for example, when the combining beam splitting mirror is optically flat and all broadening effects may be neglected. We let $A_a = 2\beta A_1 A_L$, $A_b = 2\beta A_2 A_L$, $\omega_a = \omega_1 - \omega_L$, $\omega_b = \omega_2 - \omega_L$, $\varphi_a = \varphi_1 - \varphi_L$, and $\varphi_b = \varphi_2 - \varphi_L$. The signal input to the square-law device is then

$$s(t) = s_a(t) + s_b(t) = A_a\cos(\omega_a t + \varphi_a) + A_b\cos(\omega_b t + \varphi_b). \quad (19)$$

The amplitudes A_a and A_b are, in this case, constant; the phases φ_a and φ_b are taken to be random variables uniformly distributed over the interval $(0, 2\pi)$ and independent of each other. We easily obtain

$$R_a(\tau) = E[s_{a1}s_{a2}] = A_a^2 E[\cos(\omega_a t_1 + \varphi_a)\cos(\omega_a t_2 + \varphi_a)] = \frac{1}{2}A_a^2\cos\omega_a\tau, \quad (20)$$

with $\tau = t_1 - t_2$. Similarly

$$R_b(\tau) = E[s_{b1}s_{b2}] = \frac{1}{2}A_b^2\cos\omega_b\tau. \quad (21)$$

The total correlation function of the input signal $R_s(\tau)$ is the sum of the individual correlation functions

$$R_s(\tau) = R_a(\tau) + R_b(\tau) = \frac{1}{2}A_a^2\cos\omega_a\tau + \frac{1}{2}A_b^2\cos\omega_b\tau. \quad (22)$$

Taking the Fourier transform, we obtain the power spectral density for the input signal,

$$S_s(f) = (A_a^2/4)[\delta(f - f_a) + \delta(f + f_a)] + (A_b^2/4)[\delta(f - f_b) + \delta(f + f_b)], \quad (23)$$

where $f_a = \omega_a/2\pi = f_1 - f_L$ and $f_b = \omega_b/2\pi = f_2 - f_L$. The shot noise arising from the strong LO is taken to be white Gaussian over the frequency band $[0, f_n]$. Thus, the noise spectrum is

$$S_n(f) = \begin{cases} N, & \text{for } 0 < |f| < f_n, \\ 0, & \text{elsewhere.} \end{cases} \quad (24)$$

The total input power spectral density $S_x(f)$ including the noise is shown in Fig. 2. We arbitrarily assume that $f_1 > f_2$, or $f_a > f_b$, and $A_b > A_a$.

B. Output Power Spectral Density

From Eq. (18), we obtain

$$R_{a\times a}(\tau) = \alpha^2 E[s_{a1}^2 s_{a2}^2] = \alpha^2 E[A_a^4\cos^2(\omega_a t_1 + \varphi_a)\cos^2(\omega_a t_2 + \varphi_a)] = (\alpha^2/4)A_a^4 + (\alpha^2/8)A_a^4\cos2\omega_a\tau. \quad (25a)$$

Similarly,

$$R_{b\times b}(\tau) = (\alpha^2/4)A_b^4 + (\alpha^2/8)A_b^4\cos2\omega_b\tau. \quad (25b)$$

Also,

$$R_{a\times b}(\tau) = 4\alpha^2 E[s_{a1}s_{a2}]E[s_{b1}s_{b2}] + 2\alpha^2\sigma_a^2\sigma_b^2 = (\alpha^2/2)A_a^2A_b^2\cos(\omega_a - \omega_b)\tau + (\alpha^2/2)A_a^2A_b^2\cos(\omega_a + \omega_b)\tau + (\alpha^2/2)A_a^2A_b^2. \quad (25c)$$

We note that because of the zero means,

$$\sigma_a^2 = R_a(0) = (A_a^2/2) \text{ and } \sigma_b^2 = R_b(0) = (A_b^2/2). \quad (26)$$

The total signal-by-signal correlation function $R_{s\times s}(\tau)$ is therefore given by

$$R_{s\times s}(\tau) = R_{a\times a}(\tau) + R_{b\times b}(\tau) + R_{a\times b}(\tau) = (\alpha^2/4)(A_a^2 + A_b^2)^2 + (\alpha^2/8)A_a^4\cos2\omega_a\tau + (\alpha^2/8)A_b^4\cos2\omega_b\tau + (\alpha^2/2)A_a^2A_b^2\cos(\omega_a - \omega_b)\tau + (\alpha^2/2)A_a^2A_b^2\cos(\omega_a + \omega_b)\tau. \quad (27)$$

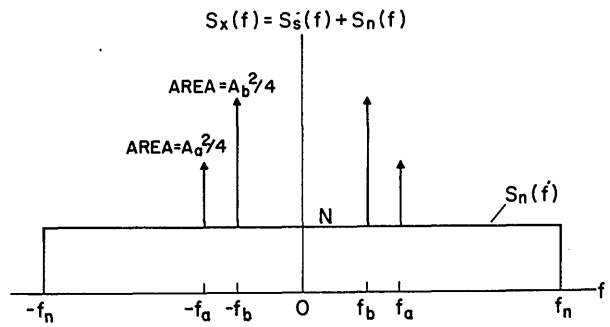

Fig. 2. The power spectral density seen at the input to the square-law device for the sinewave case. If $A_a \neq A_b$, we arbitrarily choose $A_b > A_a$, as shown above.

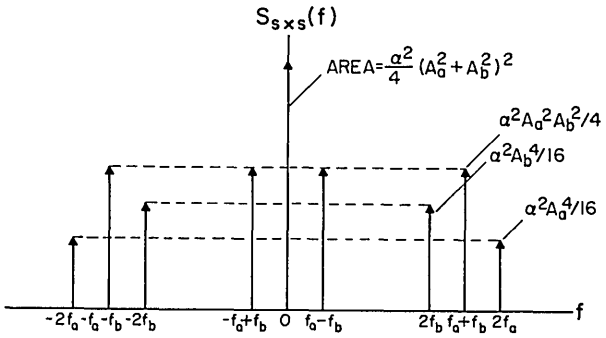

Fig. 3. The signal-by-signal power spectral density at the output of the square-law device (sinewave case).

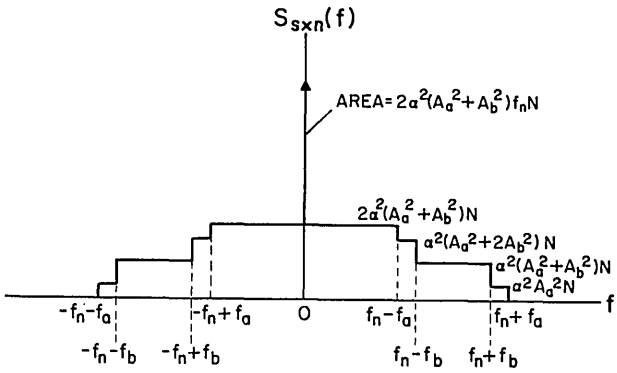

Fig. 4. The signal-by-noise power spectral density at the output of the square-law device (sinewave case).

The signal-by-signal part of the power spectral density $S_{s\times s}(f)$ is then, by taking the Fourier transform of $R_{s\times s}(\tau)$,

$$\begin{aligned} S_{s\times s}(f) &= (\alpha^2/4)(A_a^2 + A_b^2)^2\delta(f) \\ &+ [\alpha^2A_a^4/16][\delta(f - 2f_a) + \delta(f + 2f_a)] \\ &+ [\alpha^2A_b^4/16][\delta(f - 2f_b) + \delta(f + 2f_b)] \\ &+ [\alpha^2A_a^2A_b^2/4][\delta(f - f_a + f_b) + \delta(f + f_a - f_b)] \\ &+ [\alpha^2A_a^2A_b^2/4][\delta(f - f_a - f_b) + \delta(f + f_a + f_b)]. \end{aligned} \quad (28)$$

Equation (28) is shown in Fig. 3.

For the signal-by-noise part, we have from Eqs. (18e) and (18f) that

$$\begin{aligned} R_{s\times n}(\tau) &= R_{a\times n}(\tau) + R_{b\times n}(\tau) \\ &= 4\alpha^2R_n(\tau)[R_a(\tau) + R_b(\tau)] + 2\alpha^2\sigma_n^2(\sigma_a^2 + \sigma_b^2) \\ &= 2\alpha^2A_a^2R_n(\tau)\cos\omega_a\tau \\ &+ 2\alpha^2A_b^2R_n(\tau)\cos\omega_b\tau + \alpha^2(A_a^2 + A_b^2)\sigma_n^2 . \end{aligned} \quad (29)$$

The corresponding power spectral density is then

$$\begin{aligned} S_{s\times n}(f) &= \alpha^2A_a^2[S_n(f - f_a) + S_n(f + f_a)] \\ &+ \alpha^2A_b^2[S_n(f - f_b) + S_n(f + f_b)] + \alpha^2(A_a^2 + A_b^2)\sigma_n^2\delta(f), \end{aligned} \quad (30)$$

where $S_n(f - f_0)$ indicates that f_0 replaces 0 as the center frequency. This spectral density is plotted in Fig. 4.

Since

$$R_{n^2}(\tau) = 2R_n^2(\tau) + \sigma_n^4$$

for Gaussian noise,[19] Eq. (18c) for the noise-by-noise part becomes

$$R_{n\times n}(\tau) = 2\alpha^2R_n^2(\tau) + \alpha^2\sigma_n^4 , \quad (31)$$

whence

$$S_{n\times n}(f) = 2\alpha^2\int_{-\infty}^{\infty} S_n(f')S_n(f - f')df' + \alpha^2\sigma_n^4\delta(f). \quad (32)$$

For the input noise spectrum described by Eq. (24), we have

$$\sigma_n^2 = \int_{-\infty}^{\infty} S_n(f)df = 2f_nN. \quad (33)$$

Equation (32) can therefore be simplified to

$$S_{n\times n}(f) = 4\alpha^2f_n^2N^2\delta(f) + \begin{cases} 2\alpha^2N^2(2f_n - |f|), & \text{for } |f| < 2f_n, \\ 0, & \text{elsewhere,} \end{cases} \quad (34)$$

which is shown in Fig. 5.

The total output power spectral density $S_y(f)$ is the sum of $S_{s\times s}(f)$, $S_{s\times n}(f)$, and $S_{n\times n}(f)$ and is plotted in Fig. 6, where we have assumed that $f_c = f_a - f_b = f_1 - f_2$ lies in the region between the origin and $f_n - f_a$. In fact, f_c could be anywhere over the band f_n. We will consider two extreme cases: (a) $0 < f_c < f_n - f_a$ and (b) $f_n - f_b < f_c < f_n$.

C. Final Output Signal-to-Noise Ratio

Since $f_c = f_a - f_b$ is known with great accuracy, we can place a bandpass filter, with center frequency f_c, after the square-law device and obtain an output signal at this frequency. We wish to obtain the output signal-to-noise ratio $(SNR)_o$ in terms of the input signal-to-noise ratio $(SNR)_i = (SNR)_{power}$ for the two extreme cases indicated in the previous section.

From Eq. (28) along with Fig. 3 (or Fig. 6), we see that the output signal power S_o at the frequency f_c is

$$S_o = \alpha^2A_a^2A_b^2/2. \quad (35)$$

For a bandpass filter with bandwidth B, and for $0 < f_c < f_n - f_a$, the output noise power is the area under

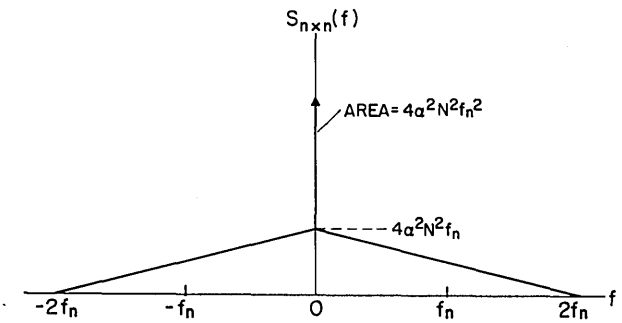

Fig. 5. The noise-by-noise power spectral density at the output of the square-law device.

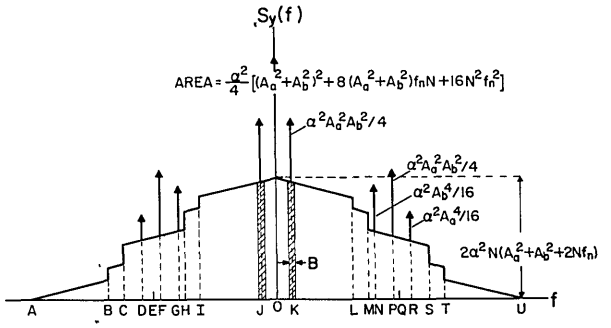

Fig. 6. The total power spectral density at the output of the square-law device for the sinewave case (not to scale). Correspondence between letters in figure and abscissa frequencies are (A) $-2f_n$, (B) $-f_n - f_a$, (C) $-f_n - f_b$, (D) $-2f_a$, (E) $-f_n$, (F) $-f_a - f_b$, (G) $-2f_b$, (H) $-f_n + f_b$, (I) $-f_n + f_a$, (J) $-f_a + f_b$, (K) $f_a - f_b$, (L) $f_n - f_a$, (M) $f_n - f_b$, (N) $2f_b$, (P) $f_a + f_b$, (Q) f_n, (R) $2f_a$, (S) $f_n + f_b$, (T) $f_n + f_a$, and (U) $2f_n$. The cross-hatched area represents the final bandpass filter, of bandwidth B.

the power spectral density curve enclosed by B (see Figs. 4, 5, and 6), which we choose to be rectangular for simplicity. Although strictly speaking, the rectangular function B (as well as Δf) is not realizable, this is not critical since it is the integrated area under the curve that is important rather than the detailed shape. The result is

$$N_o = 4\alpha^2NB(A_a^2 + A_b^2) + 4\alpha^2N^2B(2f_n - f_a + f_b), \quad 0 < f_c < f_n - f_a. \tag{36}$$

The first term is due to the $s \times n$ interaction, and the second term is due to the $n \times n$ interaction. Equation (36) can also be obtained from Eqs. (30) through (34).

The final signal-to-noise ratio at the output of the bandpass filter for this first case is therefore given by

$$(\mathrm{SNR})_o = \frac{S_o}{N_o} = \frac{A_a^2A_b^2}{8NB[(A_a^2 + A_b^2) + N(2f_n - f_a + f_b)]}, \quad 0 < f_c < f_n - f_a. \tag{37}$$

The input signal power S_i and noise power N_i are, from Fig. 2,

$$S_i = R_s(0) = \tfrac{1}{2}(A_a^2 + A_b^2), \tag{38a}$$

$$N_i = \sigma_n^2 = 2f_nN. \tag{38b}$$

Thus, in terms of the input signal-to-noise ratio $(\mathrm{SNR})_i = S_i/N_i = (A_a^2 + A_b^2)/4f_nN$, Eq. (37) can be written as

$$(\mathrm{SNR})_o = k_P(\mathrm{SNR})_i^2 \Big/ \left[\left(1 - \frac{f_a - f_b}{2f_n}\right) + 2(\mathrm{SNR})_i\right], \quad 0 < f_c < f_n - f_a, \tag{39}$$

with

$$k_P = f_nA_a^2A_b^2/[B(A_a^2 + A_b^2)^2]. \tag{40}$$

The output signal-to-noise ratio is therefore inversely proportional to B, indicating that a small value for the final bandwidth is desired. Actually, B should be chosen much smaller than f_n so the above results can be exactly correct, although results for an arbitrary value of B can easily be obtained from Fig. 6 and its associated equations.

If $f_c = f_a - f_b \to 0$, the minimum value for $(\mathrm{SNR})_o$ is obtained:

$$(\mathrm{SNR})_o^{\min} = k_P(\mathrm{SNR})_i^2/[1 + 2(\mathrm{SNR})_i]. \tag{41}$$

A log plot of Eq. (41) is shown in Fig. 7. Since $(\mathrm{SNR})_o$ will increase as f_c increases, the curve will be shifted up as f_c increases from zero. The degenerate case $f_a \equiv f_b$ should be avoided in practice because of additional noise contributions.

We now consider the second case, where $f_n - f_b < f_c < f_n$. Following the same procedure as above, we obtain

$$N_o = 2\alpha^2NB(A_a^2 + A_b^2) + 4\alpha^2N^2B(2f_n - f_a + f_b), \quad f_n - f_b < f_c < f_n, \tag{42}$$

and

$$(\mathrm{SNR})_o = k_P(\mathrm{SNR})_i^2 \Big/ \left[\left(1 - \frac{f_a - f_b}{2f_n}\right) + (\mathrm{SNR})_i\right], \quad f_n - f_b < f_c < f_n. \tag{43}$$

If we choose $f_c = f_a - f_b = f_n$, a maximum value for the $(\mathrm{SNR})_o$ is obtained:

$$(\mathrm{SNR})_o^{\max} = 2k_P(\mathrm{SNR})_i^2/[1 + 2(\mathrm{SNR})_i]. \tag{44}$$

The log plot of Eq. (44) is also given in Fig. 7; the result is the $(\mathrm{SNR})_o^{\min}$ curve shifted vertically upward by log 2. It now becomes clear that, for intermediate cases, i.e., $0 < f_c < f_n$, the $(\mathrm{SNR})_o$ curve will lie in between the curves $(\mathrm{SNR})_o^{\min}$ and $(\mathrm{SNR})_o^{\max}$. Thus, from a signal-to-noise ratio point of view, it is preferable to maintain the known difference frequency $\Delta\nu$

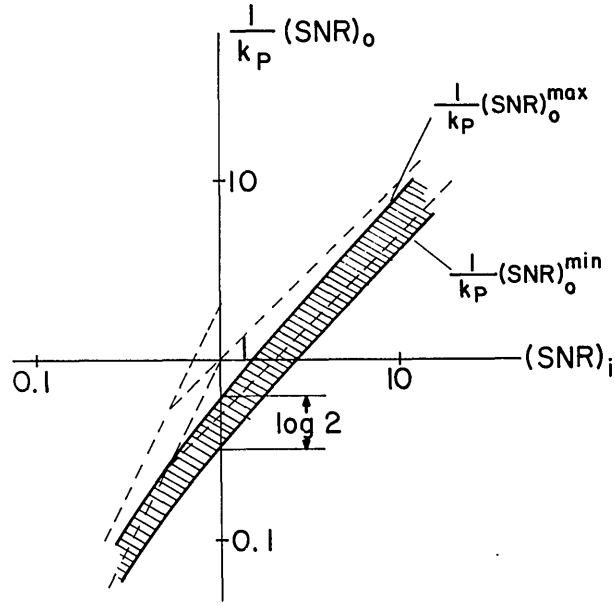

Fig. 7. The $(1/k_P)(\mathrm{SNR})_o$ vs $(\mathrm{SNR})_i$ curve. The actual signal-to-noise ratio depends on the relative values of $(f_a - f_b)$ and f_n, and lies in the shaded region. This curve also applies to the Gaussian signal case, provided that the quantity k_P is replaced by k_G or k_L, for Gaussian and Lorentzian spectra, respectively (see text).

at a maximum value close to f_n. For all cases, decreasing B will always yield improvement.

We can easily show that equal received power in each beam leads to optimum operation. From Eq. (40), we see that $k_P \propto A_a^2 A_b^2/(A_a^2 + A_b^2)^2$. Because of the symmetry between A_a and A_b, we maximize k_P by calculating the derivative

$$(\partial k_P/\partial A_a)\big|_{A_b=\text{const}} = 0.$$

This leads to the relation $A_a = A_b$.

VI. Discussion of Results for the Output Signal-to-Noise Ratio (Sinewave Case)

From Eqs. (41) and (44), the output signal-to-noise ratio $(\text{SNR})_o$ is seen to be bounded as follows:

$$k_P(\text{SNR})_i^2/[1 + 2(\text{SNR})_i] \le (\text{SNR})_o \le 2k_P(\text{SNR})_i^2/[1 + 2(\text{SNR})_i]. \quad (45)$$

If we examine the specific (and optimum) case of $A_a = A_b$ so that $k_P = f_n/4B$, with $(\text{SNR})_i = \eta P_r/h\nu f_n$ as given by Eq. (10b), we obtain

$$\frac{f_n}{4B}\left[\frac{(\eta P_r/h\nu f_n)^2}{1 + 2\eta P_r/h\nu f_n}\right] \le (\text{SNR})_o \le \frac{f_n}{2B}\left[\frac{(\eta P_r/h\nu f_n)^2}{1 + 2\eta P_r/h\nu f_n}\right]. \quad (46)$$

This yields an approximate average value given by

$$(\text{SNR})_o \simeq \frac{f_n}{3B}\left[\frac{(\eta P_r/h\nu f_n)^2}{1 + 2\eta P_r/h\nu f_n}\right]. \quad (47)$$

To obtain the minimum detectable power ${}^3P_r(\text{min})$ for this three-frequency system, we set $(\text{SNR})_o = 1$ and solve for P_r. Thus,

$$\eta\frac{{}^3P_r(\text{min})}{h\nu f_n} = \frac{3B}{f_n} + \left\{\frac{3B}{f_n}\left(1 + \frac{3B}{f_n}\right)\right\}^{1/2}. \quad (48a)$$

Since $B \ll f_n$,

$$\eta\,{}^3P_r(\text{min})/h\nu f_n \simeq 3B/f_n + (3B/f_n)^{1/2}(1 + 3B/2f_n) \simeq \left(\frac{3B}{f_n}\right)^{1/2} \quad (48b)$$

and therefore

$${}^3P_r(\text{min}) \simeq (3Bf_n)^{1/2}(h\nu/\eta) = (3B/f_n)^{1/2}P_r(\text{min}), \quad (49)$$

with $P_r(\text{min}) = f_n h\nu/\eta$ as the standard minimum detectable power for the conventional heterodyne system with Doppler uncertainty f_n.[2,3,8] By choosing $B \ll f_n$, therefore, it is possible to achieve a reduced minimum detectable power

$${}^3P_r(\text{min}) \ll P_r(\text{min}), \quad B \ll f_n \quad (50)$$

using three-frequency nonlinear heterodyne detection. *Equations (45)–(50) represent the key results obtained in this analysis.*

In the limit of large $(\text{SNR})_i$ (strong input signals and/or small Doppler uncertainty), $P_r/f_n \gg h\nu/\eta$ and Eq. (46) yields the relationship

$$\eta P_r/8h\nu B \le (\text{SNR})_o \le \eta P_r/4h\nu B. \quad (51)$$

This can be approximated, then, as

$${}^3(\text{SNR})_{\text{power}} \simeq \eta P_r/6h\nu B = (f_n/6B)\left(\frac{\eta P_r}{h\nu f_n}\right) = (f_n/6B)(\text{SNR})_{\text{power}}, \quad (52)$$

where $(\text{SNR})_{\text{power}} = \eta P_r/h\nu f_n$ is the signal-to-noise ratio for the conventional heterodyne system as given in Eq. (10b). Again, we can provide that

$${}^3(\text{SNR})_{\text{power}} \gg (\text{SNR})_{\text{power}} \quad (53)$$

by choosing $B \ll f_n$.

VII. Application to Radiowave and Microwave Frequencies

Thus far, we have been especially concerned with absorption detectors operating in the optical and ir regions of the electromagnetic spectrum ($h\nu \gg kT$, where k is the Boltzmann constant and T is the detector temperature). In this case, the intensity of the incoming wave is obtained from the analytic signal and excludes double- and sum-frequency components.[5,11,15,16] Nevertheless, Eq. (45) is a general result for intensity detection that applies also to the microwave and radiowave regions ($h\nu \ll kT$).

For low frequencies, the intensity is related to the square of the electric field, $I \propto E^2$. For a diode mixer that is either operating in the square-law regime, or in the linear regime followed by a square-law device, the detector response r for a three-frequency system is then given by the classical expression

$$\begin{aligned} r = \beta' E_t^2 &= \beta'[A_1\cos(\omega_1 t + \varphi_1) + A_2\cos(\omega_2 t + \varphi_2) + A_L\cos(\omega_L t + \varphi_L)]^2 \\ &= \beta'\{A_1^2\cos^2(\omega_1 t + \varphi_1) + A_2^2\cos^2(\omega_2 t + \varphi_2) + A_L^2\cos^2(\omega_L t + \varphi_L) + A_1A_2\cos[(\omega_1 - \omega_2)t + (\varphi_1 - \varphi_2)] \\ &+ A_1A_2\cos[(\omega_1 + \omega_2)t + (\varphi_1 + \varphi_2)] + A_1A_L\cos[(\omega_1 - \omega_L)t + (\varphi_1 - \varphi_L)] + A_1A_L\cos[(\omega_1 + \omega_L)t + (\varphi_1 + \varphi_L)] \\ &+ A_2A_L\cos[(\omega_2 - \omega_L)t + (\varphi_2 - \varphi_L)] + A_2A_L\cos[(\omega_2 + \omega_L)t + (\varphi_2 + \varphi_L)]\}. \end{aligned} \quad (54)$$

Note that $A^2\cos^2(\omega t + \varphi) = (A^2/2)[1 + \cos(2\omega t + 2\varphi)]$. Now, since the detector generally does not follow the instantaneous intensity at double- and sum-frequencies ($2\omega_1$, $\omega_1 + \omega_2$, ...), only dc and difference-frequency terms remain. Hence Eq. (54) will in practice reduce to Eq. (4). The calculations leading to Eq. (45) will remain correct, provided, of course, that we insert the proper relation for $(\text{SNR})_i$ in the classical low frequency detection regime. Generally, this is obtained by replacing $h\nu$ by kT and η by $1/F_T$, where F_T is the noise figure of the receiver.

Once the target is ascertained to be present, a wide bandpass filter can be gradually narrowed about $2|f_1' - f_L|$ or $2|f_2' - f_L|$ and thereby used to obtain Doppler information. Alternatively one could, of course, switch to a conventional configuration.

VIII. Operation in Other Configurations

It is of interest to examine the operation of the three-frequency nonlinear heterodyne system in a variety of configurations[20] different from those as-

sumed earlier. In this section, we consider the behavior of the system under the following conditions: (1) at zero frequency (dc), (2) without a final bandpass filter, (3) with increased Doppler information, (4) as an optimum system with no uncertainty in Doppler shift, and (5) with a νth-law nonlinear device other than square-law. We also consider consequences of four-frequency nonlinear heterodyne detection.

Assuming that $B \rightarrow 0$, a calculation of $(\mathrm{SNR})_o$ for the final filter centered at zero frequency rather than at f_c yields the result given by Eq. (41) with $k_P = 1$, thus independent of f_n, A_a, A_b, and B. The advantageous factor f_n/B therefore does not appear in the equation. For $B > 0$, the noise increases while the signal does not, thus the above result is optimum for zero frequency. It must be kept in mind, however, that this result has been obtained for a system containing a blocking capacitor (see Fig. 1).

If we altogether omit the final bandpass filter, a rather complicated expression for $(\mathrm{SNR})_o$ obtains. Assuming that f_a and f_b are much smaller than f_n, and with $A_a = A_b$, the MDP is calculated to be ${}^3P_r(\min) \simeq 2.9\, h\nu f_n/\eta$, approximately a factor of three worse than the conventional system.

We now consider the case in which the bandpass filter barely encompasses f_a and f_b, so $f_i = f_b$ and $f_n = f_a$, with $f_a > f_b$. Clearly, decreasing this bandwidth should decrease the over-all noise and thereby improve system performance, but this requires knowledge of the Doppler shifts involved. A calculation of the average MDP yields the results ${}^3P_r(\min) \simeq 3h\nu B/\eta$, which is considerably lower than the result given in Eq. (49), as it should be.

A calculation for the case in which complete Doppler information is available displays clearly the additional noise introduced by the three-frequency system over the conventional system by virtue of the nonlinear processing. The result for the MDP in this case is ${}^3P_r(\min) \simeq 1.8\, h\nu B/\eta$, which is a factor of 1.8 greater than the MDP for the conventional heterodyne receiver with bandwidth B.

General considerations[21] show that all νth-law detectors behave in an essentially similar manner to the full-wave square-law detector in terms of the ratio of $(\mathrm{SNR})_o$ and $(\mathrm{SNR})_i$. For large values of $(\mathrm{SNR})_i$, therefore, $(\mathrm{SNR})_o$ is expected to be directly proportional to $(\mathrm{SNR})_i$. Thus, if a half-wave linear device were used instead of the full-wave square-law device considered previously, we would expect results similar to those obtained earlier. This provides a wide choice for designing a heterodyne nonlinear detector combination, perhaps in a single package.

Finally, we consider the consequences of four-frequency mixing. This would have the advantage of making the transmitter and LO identical. Assuming that only one of the sidebands of the LO is strong (A_{L1}), the $(\mathrm{SNR})_o$ is still given by Eqs. (41) and (44), but in this case

$$ {}^4k_P = f_n A_a^2 A_b^2/[B(A_a^2 + A_b^2 + A_c^2)^2], \qquad (55) $$

with $A_c/A_a = A_{L2}/A_1$. If $A_1 = A_2 = A_{L2}$, we obtain ${}^4k_P = f_n/9B$, which is to be compared with the value ${}^3k_P = f_n/4B$ for the three-frequency case. Thus a single unit may be used both as transmitter and local oscillator without a great deal of loss, provided that one of the two sidebands of the LO beam is attenuated down to the level of the received signal. From Eq. (55), it is seen that the LO optimally consists of a single frequency, however.

The worst case, in which the LO consists of two strong frequencies separated by f_c, gives rise to very large $s \times n$ terms arising from the beating between the two LO frequencies. Aside from other terms not contained in Eq. (55), this case would make the $A_c{}^4$ term in the denominator of Eq. (55) very large, leading to a factor $(P_r/P_L)^2$ in $(\mathrm{SNR})_o$ (P_r and P_L are typical signal and LO powers, respectively.) Thus, in other than very large input SNR situations, the transmitter cannot be directly used as an LO without attenuation of one of its sidebands.

IX. Gaussian Input Signals with Gaussian Spectra

The sinusoidal signal assumption is, in many cases, an idealization that provides simple physical and mathematical insights into a problem. In most real situations, however, the heterodyne signal will have a narrowband character.[2-5,11] This may be due to the surface roughness of a scattering target in a radar system or due to the modulation imposed on the carrier in a communications system. For a scatterer returning Gaussian radiation, experiments show that the power spectral density is also frequently in the Gaussian form.[4,5,22,23] It is the purpose of this section to investigate this case.

We assume that the two signal inputs to the photodetector, $E_1(t)$ and $E_2(t)$, take the form of narrowband Gaussian processes:

$$ E_1(t) = A_1(t)\cos(\omega_1 t + \varphi_1), \qquad (56a) $$

$$ E_2(t) = A_2(t)\cos(\omega_2 t + \varphi_2), \qquad (56b) $$

where, for any given t, the two independent amplitudes $A_1(t)$ and $A_2(t)$ are random variables with Rayleigh distributions and the two independent phases φ_1 and φ_2 are uniformly distributed over the interval $(0, 2\pi)$. It should be noted that the independent amplitude case considered here is appropriate only for a sufficiently large value of $\Delta\nu$ and for sufficiently large targets. After mixing with a stable LO and filtering out the dc portion, the signal input to the square-law device is easily found to be[4,5,11]

$$ s(t) = 2\beta A_L A_1(t)\cos[(\omega_1 - \omega_L)t + (\varphi_1 - \varphi_L)] + 2\beta A_L A_2(t)\cos[(\omega_2 - \omega_L)t + (\varphi_2 - \varphi_L)]. \qquad (57) $$

Since β and A_L are constant, the new amplitudes $A_a(t) = 2\beta A_L A_1(t)$ and $A_b(t) = 2\beta A_L A_2(t)$ remain Rayleigh distributed. Similarly, the new phases $\varphi_a = \varphi_1 - \varphi_L$ and $\varphi_b = \varphi_2 - \varphi_L$ can be easily shown to possess uniform distributions over $(0, 2\pi)$. Therefore the narrowband Gaussian nature of the signals is preserved, provided that the envelope variations are slower than the intermediate frequencies $\omega_1 - \omega_L$ and $\omega_2 - \omega_L$,[4,5,11] and we write

$$s(t) = A_a(t)\cos(\omega_a t + \varphi_a) + A_b(t)\cos(\omega_b t + \varphi_b). \quad (58)$$

A. Input Power Spectral Density

The power spectral densities for the narrowband Gaussian inputs are also taken to be Gaussian. Thus

$$S_s(f) = S_a(f) + S_b(f), \quad (59a)$$

with

$$S_a(f) = P_a\exp[-(f - f_a)^2/2\gamma_a{}^2] + P_a\exp[-(f + f_a)^2/2\gamma_a{}^2], \quad (59b)$$

$$S_b(f) = P_b\exp[-(f - f_b)^2/2\gamma_b{}^2] + P_b\exp[-(f + f_b)^2/2\gamma_b{}^2], \quad (59c)$$

where P_a and P_b represent the peak values of the Gaussian distributions, and γ_a and γ_b are their standard deviations. The signal powers are then given by

$$\sigma_a{}^2 = \int_{-\infty}^{\infty} S_a(f)df = 2(2\pi)^{1/2}\gamma_a P_a = \langle A_a{}^2\rangle/2, \quad (60a)$$

$$\sigma_b{}^2 = \int_{-\infty}^{\infty} S_b(f)df = 2(2\pi)^{1/2}\gamma_b P_b = \langle A_b{}^2\rangle/2. \quad (60b)$$

The noise input once again is assumed to be white Gaussian over the real frequency band $[0, f_n]$ and therefore has the same spectral density as the sinewave input case. The total power spectral density at the input to the square-law device is presented in Fig. 8 (compare with Fig. 2 for the sinewave case).

B. Output Power Spectral Density

Because the signals are stationary Gaussian processes, the signal-by-signal correlation functions at the output of the square-law device are given by [see Eq. (31)]

$$R_{a\times a}(\tau) = 2\alpha^2 R_a{}^2(\tau) + \alpha^2\sigma_a{}^4, \quad (61a)$$

$$R_{b\times b}(\tau) = 2\alpha^2 R_b{}^2(\tau) + \alpha^2\sigma_b{}^4. \quad (61b)$$

From Eq. (32), the Fourier transform of $R_{a\times a}(\tau)$ is

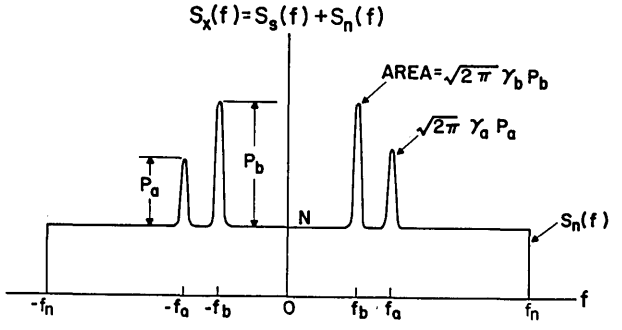

Fig. 8. The power spectral density at the input to the square-law device for the Gaussian signal case. We arbitrarily choose $P_b > P_a$, as seen above.

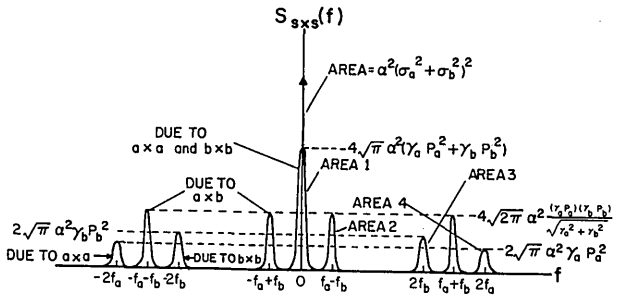

Fig. 9. The signal-by-signal power spectral density at the output of the square-law device (Gaussian signal case). Areas under curves:
Area 1 = $8\pi\alpha^2(\gamma_a{}^2P_a{}^2 + \gamma_b{}^2P_b{}^2)$;
Area 2 = $8\pi\alpha^2(\gamma_a P_a)(\gamma_b P_b)$;
Area 3 = $4\pi\alpha^2\gamma_b{}^2P_b{}^2$;
Area 4 = $4\pi\alpha^2\gamma_a{}^2P_a{}^2$.

$$S_{a\times a}(f) = 2\alpha^2\int_{-\infty}^{\infty} S_a(f')S_a(f - f')df' + \alpha^2\sigma_a{}^4\delta(f)$$

$$= 2(\pi)^{1/2}\alpha^2\gamma_a P_a{}^2\left[e^{-(f-2f_a)^2/4\gamma_a{}^2} + e^{-(f+2f_a)^2/4\gamma_a{}^2} + 2e^{-f^2/4\gamma_a{}^2}\right] + \alpha^2\sigma_a{}^4\delta(f), \quad (62)$$

with the identical result for $S_{b\times b}(f)$ (b replaces a). Furthermore, using Eq. (18d), we obtain

$$S_{a\times b}(f) = 4(2\pi)^{1/2}\alpha^2\frac{(\gamma_a P_a)(\gamma_b P_b)}{(\gamma_a{}^2+\gamma_b{}^2)^{1/2}}\left(\exp\left\{-\frac{[f-(f_a+f_b)]^2}{2(\gamma_a{}^2+\gamma_b{}^2)}\right\} + \exp\left\{-\frac{[f+(f_a+f_b)]^2}{2(\gamma_a{}^2+\gamma_b{}^2)}\right\} + \exp\left\{-\frac{[f-(f_a-f_b)]^2}{2(\gamma_a{}^2+\gamma_b{}^2)}\right\} + \exp\left\{-\frac{[f+(f_a-f_b)]^2}{2(\gamma_a{}^2+\gamma_b{}^2)}\right\}\right) + 2\alpha^2\sigma_a{}^2\sigma_b{}^2\delta(f). \quad (63)$$

The total signal-by-signal power spectral density $S_{s\times s}(f)$ is, of course, given by

$$S_{s\times s}(f) = S_{a\times a}(f) + S_{b\times b}(f) + S_{a\times b}(f), \quad (64)$$

and is shown in Fig. 9 (compare with Fig. 3 for the sinewave case).

For the signal-by-noise part, we have

$$R_{s\times n}(\tau) = R_{a\times n}(\tau) + R_{b\times n}(\tau), \quad (65)$$

and, from Eq. (18e), we write

$$R_{a\times n}(\tau) = 4\alpha^2 R_a(\tau)R_n(\tau) + 2\alpha^2\sigma_a{}^2\sigma_n{}^2, \quad (66)$$

which Fourier transforms to

$$S_{a\times n}(f) = 4\alpha^2\int_{-\infty}^{\infty} S_a(f')S_n(f - f')df + 2\alpha^2\sigma_a{}^2\sigma_n{}^2\delta(f). \quad (67)$$

This can be readily evaluated to yield

$$S_{a\times n}(f) = 4(2\pi)^{1/2}\alpha^2 NP_a\gamma_a\{\Phi[(f + f_n - f_a)/\gamma_a] - \Phi[(f - f_n - f_a)/\gamma_a] + \Phi[(f + f_n + f_a)/\gamma_a] - \Phi[(f - f_n + f_a)/\gamma_a]\} + 2\alpha^2\sigma_a{}^2\sigma_n{}^2\delta(f), \quad (68)$$

where $\Phi[x]$ is the normal distribution function

$$\Phi[x] = (2\pi)^{-1/2}\int_{-\infty}^{x} e^{-x'^2/2}dx'. \quad (69)$$

Similarly, we obtain the identical result for $S_{b\times n}$ (b replaces a). The total signal-by-noise power spectral

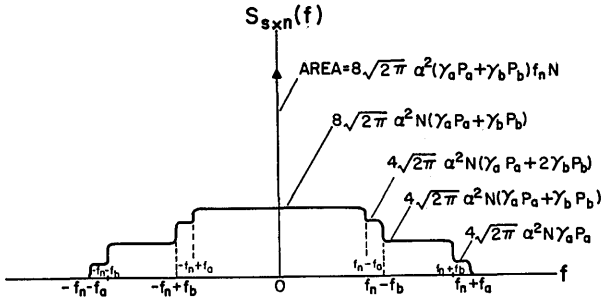

Fig. 10. The signal-by-noise power spectral density at the output of the square-law device (Gaussian signal case).

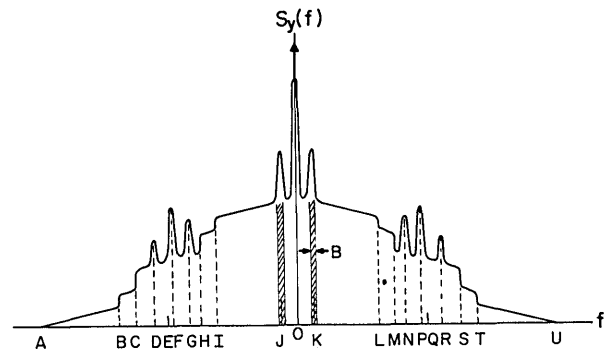

Fig. 11. The total power spectral density at the output of the square-law device for the Gaussian signal case. Note the smoothing of all sharp edges. This figure is similar to Fig. 6 except that the delta functions are replaced by Gaussians.

density $S_{s\times n}(f)$ is just the sum of $S_{a\times n}(f)$ and $S_{b\times n}(f)$, or

$$S_{s\times n}(f) = S_{a\times n}(f) + S_{b\times n}(f). \tag{70}$$

A sketch of $S_{s\times n}(f)$ is given in Fig. 10. Assuming that the standard deviations γ_a and γ_b are small in comparison with the width of the plateau regions in Fig. 4, the plot will be very similar to that of the sinewave case. The only notable difference is the rounding of sharp corners. Small values of γ_a and γ_b also guard against spectrum overlap, which would make the solution of the problem more difficult.

The noise-by-noise power spectral density is the same as that for the pure sinewave case (Fig. 5). The total output power spectral density $S_y(f)$ is plotted in Fig. 11, where we arbitrarily have assumed that $f_a > f_b$ and $f_a - f_b < f_n - f_a < f_n$.

C. Final Output Signal-to-Noise Ratio

Here again, we place a bandpass filter of bandwidth B and center frequency $f_c = f_a - f_b$ after the square-law device. Referring to Fig. 9 and Eq. (63), we find

$$S_o = \frac{8\alpha^2(2\pi)^{1/2}(\gamma_a P_a)(\gamma_b P_b)}{(\gamma_a^2+\gamma_b^2)^{1/2}}\left\{\int_{-B/2}^{B/2} e^{-f^2/2(\gamma_a^2+\gamma_b^2)}df\right\}$$

$$= 16\pi\alpha^2(\gamma_a P_a)(\gamma_b P_b)\left[2\Phi\left(\frac{B}{2(\gamma_a^2+\gamma_b^2)^{1/2}}\right)-1\right]. \tag{71}$$

The input signal power is, from Eq. (60), given by

$$S_i = 2(2\pi)^{1/2}(\gamma_a P_a + \gamma_b P_b). \tag{72}$$

The input noise power is the same as for the sinewave case. Referring to Figs. 5 and 10, the output noise power can be well approximated by

$$N_o = 16(2\pi)^{1/2}\alpha^2 NB(\gamma_a P_a + \gamma_b P_b) + 4\alpha^2 N^2 B(2f_n - f_a + f_b),$$
$$0 < f_a - f_b < f_n - f_a, \tag{73a}$$

$$N_o = 8(2\pi)^{1/2}\alpha^2 NB(\gamma_a P_a + \gamma_b P_b) + 4\alpha^2 N^2 B(2f_n - f_a + f_b),$$
$$f_n - f_b < f_a - f_b < f_n. \tag{73b}$$

The input signal-to-noise ratio $(\mathrm{SNR})_i$ is simply

$$(\mathrm{SNR})_i = [(2\pi)^{1/2}/Nf_n](\gamma_a P_a + \gamma_b P_b), \tag{74}$$

and the output signal-to-noise ratio $(\mathrm{SNR})_o$ can be easily evaluated:

$$(\mathrm{SNR})_o = k_G(\mathrm{SNR})_i^2\Big/\left[\left(1-\frac{f_a-f_b}{2f_n}\right)+2(\mathrm{SNR})_i\right],$$
$$0 < f_a - f_b < f_n - f_a, \tag{75a}$$

$$(\mathrm{SNR})_o = k_G(\mathrm{SNR})_i^2\Big/\left[\left(1-\frac{f_a-f_b}{2f_n}\right)+(\mathrm{SNR})_i\right],$$
$$f_n - f_b < f_a - f_b < f_n. \tag{75b}$$

These equations are identical to Eqs. (39) and (43) with the exception that the factor k_P [Eq. (40)] has been replaced by the factor k_G given by

$$k_G = \frac{f_n}{2(\gamma_a^2+\gamma_b^2)^{1/2}}\frac{(\gamma_a P_a)(\gamma_b P_b)}{(\gamma_a P_a+\gamma_b P_b)^2}\left\{\frac{1}{u}[2\Phi(u)-1]\right\}, \tag{76a}$$

with

$$u = B/[2(\gamma_a^2+\gamma_b^2)^{1/2}]. \tag{76b}$$

Now, if $f_a - f_b \to 0$ in Eq. (75a), and choosing $f_a - f_b = f_n$ in Eq. (75b), we obtain the following bounds for $(\mathrm{SNR})_o$:

$$(\mathrm{SNR})_o^{\min} = k_G(\mathrm{SNR})_i^2/[1+2(\mathrm{SNR})_i], \tag{77a}$$

$$(\mathrm{SNR})_o^{\max} = 2k_G(\mathrm{SNR})_i^2/[1+2(\mathrm{SNR})_i], \tag{77b}$$

in analogy with Eqs. (41) and (44). The results presented in Fig. 7 are therefore also appropriate to this case with the substitution of k_G for k_P.

X. Discussion of Results for the Output Signal-to-Noise Ratio (Gaussian Case)

Since $(\mathrm{SNR})_i$ is the same for the Gaussian case as it is for the pure sinewave case,[11] the results presented in Sec. VI apply directly with the simple replacement of k_P by k_G; thus

$$\frac{1}{B} \to \frac{1}{2(\gamma_a^2+\gamma_b^2)^{1/2}}\left\{\frac{1}{u}[2\Phi(u)-1]\right\} = \frac{2\Phi(u)-1}{B}, \tag{78a}$$

with

$$A_a^2 \to 4(2\pi)^{1/2}\gamma_a P_a, \tag{78b}$$

$$A_b^2 \to 4(2\pi)^{1/2}\gamma_b P_b. \tag{78c}$$

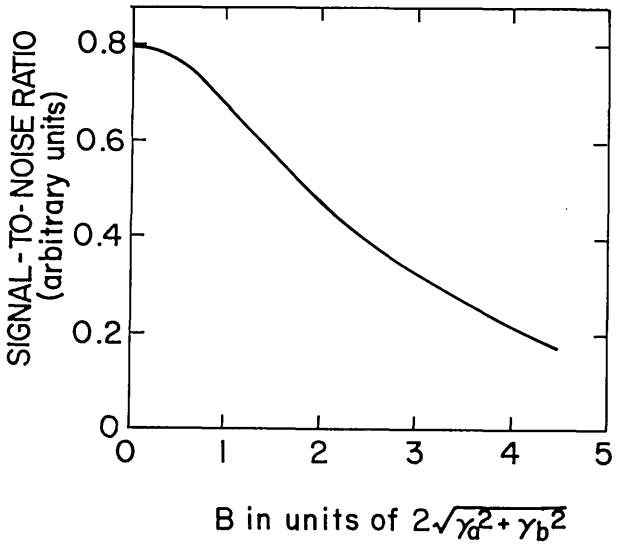

Fig. 12. Plot of the function $z(u)$ vs u, which represents the B dependence of the signal-to-noise ratio for Gaussian signals.

For equal powers in both beams, therefore, the final signal-to-noise ratio for the Gaussian case is degraded in comparison with the sinewave case by the factor $[2\Phi(u) - 1] = [\Phi(u) - \Phi(-u)] < 1$. It is clear that the spectral width, as determined by the quantity $(\gamma_a^2 + \gamma_b^2)^{1/2}$, should be minimized if possible.

We now consider the variation of the quantity k_G with the bandwidth B, assuming that the parameters f, γ_a, γ_b, P_a, and P_b are fixed. Since $u \propto B$ and $k_G \propto (1/u)[2\Phi(u) - 1] \equiv z(u)$, it is sufficient to examine the function $z(u)$ sketched in Fig. 12. It is apparent that k_G, and therefore $(\mathrm{SNR})_o$, increases with decreasing B. This evidences the fact that the noise power decreases more rapidly than the signal power as the bandwidth B is narrowed on $f_c = f_a - f_b$. This effect can be observed in Fig. 11.

For both sinewave and Gaussian signal inputs, therefore, it is desirable to minimize B. The limitation, of course, is provided by the unequal Doppler shifts of the two input signals. For a given bandwidth B, furthermore, it is understood that all of the signal will be detected in the sinewave case, though only a portion of it will be detected in the Gaussian case.

If we let γ_a and $\gamma_b \to 0$, while keeping the power constant [i.e., $(2\pi)^{1/2}\gamma_a P_a = A_a^2/4$ and $(2\pi)^{1/2}\gamma_b P_b = A_b^2/4$], the Gaussian spectra shrink to delta functions. In this limit, we observe that

$$\lim_{\substack{\gamma_a \to 0 \\ \gamma_b \to 0}} S_o(\text{Gaussian}) = (\alpha^2 A_a^2 A_b^2/2)(2\Phi[\infty] - 1) = \alpha^2 A_a^2 A_b^2/2, \quad (79)$$

which is, as expected, the expression obtained for the output power for the sinewave case [Eq. (35)].

XI. Gaussian Input Signals with Lorentzian Spectra

In those cases where the narrowband Gaussian signal inputs possess Lorentzian power spectra rather than Gaussian power spectra, the input power spectral densities are given by

$$S_a(f) = \frac{D_a\Gamma_a}{(f - f_a)^2 + \Gamma_a^2} + \frac{D_a\Gamma_a}{(f + f_a)^2 + \Gamma_a^2}, \quad (80a)$$

$$S_b(f) = \frac{D_b\Gamma_b}{(f - f_b)^2 + \Gamma_b^2} + \frac{D_b\Gamma_b}{(f + f_b)^2 + \Gamma_b^2}. \quad (80b)$$

Here D_a and D_b are arbitrary constants, and Γ_a and Γ_b are constants reflecting the spectral width. Performing the inverse Fourier transform, the autocorrelation functions are found to be

$$R_a(\tau) = \pi D_a e^{-2\pi\Gamma_a|\tau|}\cos 2\pi f_a\tau, \quad (81a)$$

$$R_b(\tau) = \pi D_b e^{-2\pi\Gamma_b|\tau|}\cos 2\pi f_b\tau, \quad (81b)$$

and the input signal powers are given by

$$\sigma_a^2 = \int_{-\infty}^{\infty} S_a(f)df = \pi D_a = \langle A_a^2\rangle/2, \quad (82a)$$

$$\sigma_b^2 = \int_{-\infty}^{\infty} S_b(f)df = \pi D_b = \langle A_b^2\rangle/2. \quad (82b)$$

With the same noise input as considered in the previous section, and making use of Eqs. (18), (61), (67), and (81), the output power spectral densities are

$$S_{a\times a}(f) = \alpha^2\pi D_a^2\left[\frac{2\Gamma_a}{f^2 + 4\Gamma_a^2} + \frac{\Gamma_a}{(f - 2f_a)^2 + 4\Gamma_a^2} + \frac{\Gamma_a}{(f + 2f_a)^2 + 4\Gamma_a^2}\right] + \alpha^2\sigma_a^4\delta(f), \quad (83a)$$

$$S_{b\times b}(f) = S_{a\times a}(f)|_{\text{sub } a \to \text{sub } b}, \quad (83b)$$

$$S_{a\times b}(f) = \alpha^2\pi D_a D_b\left[\frac{\Gamma_a + \Gamma_b}{(f - f_a - f_b)^2 + (\Gamma_a + \Gamma_b)^2} + \frac{\Gamma_a + \Gamma_b}{(f + f_a + f_b)^2 + (\Gamma_a + \Gamma_b)^2} + \frac{\Gamma_a + \Gamma_b}{(f - f_a + f_b)^2 + (\Gamma_a + \Gamma_b)^2} + \frac{\Gamma_a + \Gamma_b}{(f + f_a - f_b)^2 + (\Gamma_a + \Gamma_b)^2}\right] + 2\alpha^2\sigma_a^2\sigma_b^2\delta(f), \quad (83c)$$

$$S_{a\times n}(f) = 4\alpha^2 N D_a \tan^{-1}\left\{\frac{4f_n\Gamma_a(f^2 + f_a^2 + \Gamma_a^2 - f_n^2)}{[(f - f_a)^2 + \Gamma_a^2 - f_n^2][(f + f_a)^2 + \Gamma_a^2 - f_n^2] - 4f_n^2\Gamma_a^2}\right\} + 2\alpha^2\sigma_a^2\sigma_n^2\delta(f), \quad (83d)$$

$$S_{b\times n}(f) = S_{a\times n}|_{\text{sub } a \to \text{sub } b}, \quad (83e)$$

with $0 < \tan^{-1}x < \pi$ (negative angles excluded). For narrow spectral widths (Γ_a, Γ_b small), it is clear that the power spectral densities for the Lorentzian case should look just about the same as those for the Gaussian case. We may simply replace $2(2\pi)^{1/2}\gamma_a P_a$ and $2(2\pi)^{1/2}\gamma_b P_b$, respectively, by πD_a and πD_b [see Eqs. (60) and (82)].

We may calculate the output signal and noise to obtain $(\mathrm{SNR})_o$ as follows. Let

$$S_o = 2\pi\alpha^2 D_a D_b \int_{-B/2}^{B/2} \frac{\Gamma_a + \Gamma_b}{f^2 + (\Gamma_a + \Gamma_b)^2}\, df$$
$$= 2\pi\alpha^2 D_a D_b \tan^{-1}\left[\frac{4B(\Gamma_a + \Gamma_b)}{4(\Gamma_a + \Gamma_b)^2 - B^2}\right], \quad (84)$$

with $0 < \tan^{-1}x < \pi$. For small B, the output noise power is

$$N_o = \int_{f_a - f_b - B/2}^{f_a - f_b + B/2} [S_{a\times n}(f) + S_{b\times n}(f) + S_{n\times n}(f)]df$$
$$+ \int_{-f_a + f_b - B/2}^{-f_a + f_b + B/2} [S_{a\times n}(f) + S_{b\times n}(f) + S_{n\times n}(f)]df$$
$$\simeq B[S_{a\times n}(f_a - f_b) + S_{a\times n}(-f_a + f_b) + S_{b\times n}(f_a - f_b)$$
$$+ S_{b\times n}(-f_a + f_b)] + 4\alpha^2 N^2 B(2f_n - f_a + f_b). \quad (85)$$

As an approximation, we use the replacements $2(2\pi)^{1/2}\gamma_a P_a \rightarrow \pi D_a$ and $2(2\pi)^{1/2}\gamma_b P_b \rightarrow \pi D_b$ in Fig. 10 to obtain

$$N_o = 8\pi\alpha^2 NB(D_a + D_b) + 4\alpha^2 N^2 B(2f_n - f_a + f_b),$$
$$0 < f_a - f_b < f_n - f_a, \quad (86a)$$

$$N_o = 4\pi\alpha^2 NB(D_a + D_b) + 4\alpha^2 N^2 B(2f_n - f_a + f_b),$$
$$f_n - f_b < f_a - f_b < f_n. \quad (86b)$$

Using an input signal-to-noise ratio $(\mathrm{SNR})_i$ [see Eq. (82)] given by

$$(\mathrm{SNR})_i = \pi(D_a + D_b)/2Nf_n, \quad (87)$$

and using Eqs. (84), (86), and (87), we find the output signal-to-noise ratio $(\mathrm{SNR})_o$ to be

$$(\mathrm{SNR})_o = k_L(\mathrm{SNR})_i^2 \Big/ \left[\left(1 - \frac{f_a - f_b}{2f_n}\right) + 2(\mathrm{SNR})_i\right],$$
$$0 < f_a - f_b < f_n - f_a, \quad (88a)$$

$$(\mathrm{SNR})_o = k_L(\mathrm{SNR})_i^2 \Big/ \left[\left(1 - \frac{f_a - f_b}{2f_n}\right) + (\mathrm{SNR})_i\right],$$
$$f_n - f_b < f_a - f_b < f_n. \quad (88b)$$

This result is therefore the same as that for both the sinewave case and the Gaussian spectrum case [see Eqs. (39), (43), and (75)], except that we now use the factor k_L given by

$$k_L = \frac{f_n}{\pi(\Gamma_a + \Gamma_b)} \frac{D_a D_b}{(D_a + D_b)^2} \left\{\frac{1}{v}\left[\tan^{-1}\left(\frac{4v}{4 - v^2}\right)\right]\right\}, \quad (89)$$

with $v = B/(\Gamma_a + \Gamma_b)$. Thus the results presented in Fig. 7 apply also to this case with k_P replaced by k_L.

For small v (small B), the quantity $4v/(4 - v^2) \simeq v$. It is not difficult to show that the behavior of the function $(\tan^{-1} v)/v$ is similar to that of $z(u)$ (see Fig. 12). The maximum value occurs at the origin, so in this case too, optimum operation occurs for $B \rightarrow 0$.

Furthermore, using the replacements $\pi D_a \rightarrow A_a^2/2$ and $\pi D_b \rightarrow A_b^2/2$ and letting Γ_a, $\Gamma_b \rightarrow 0$, Eq. (89) reduces to

$$k_L \rightarrow \frac{f_n}{B} \frac{A_a^2 A_b^2}{(A_a^2 + A_b^2)^2} \left\{\lim_{\Gamma_a + \Gamma_b \to 0} \frac{1}{\pi} \tan^{-1}\left[\frac{4B(\Gamma_a + \Gamma_b)}{4(\Gamma_a + \Gamma_b)^2 - B^2}\right]\right\}$$
$$= \frac{f_n}{B} \frac{A_a^2 A_b^2}{(A_a^2 + A_b^2)^2} = k_P. \quad (90)$$

Thus, the present case also reduces to the sinewave case as the spectral width approaches zero with the power fixed. Similarly it is clear from the above that for fixed B, the spectral width, as determined by the quantity $(\Gamma_a + \Gamma_b)$, should be minimized if possible.

XII. Numerical Example

As an example of three-frequency nonlinear heterodyne detection, we consider a CO_2 laser radar operating at 10.6 μm in the ir[5,24,25] (see Fig. 1). If we assume that we wish to acquire and track a 1-m radius satellite with a rotation rate of 1 rpm, the expected bandwidth (resulting from rotation) of the radar return is of order $4R\omega_\perp/\lambda \sim 40$ kHz.[4] We therefore choose a difference frequency, f_c, at a (convenient) value of 1 MHz, which eliminates spectrum overlap. If the satellite has a radial velocity $\sim$ 10 km/sec, the Doppler frequency is $\sim$ 2GHz, yielding a value $f_c' - f_c = 2v_\parallel f_c/c \sim 60$ Hz. This shift is very small indeed compared with general frequency modulations in an ordinary heterodyne system, justifying the assumption that $f_c' - f_c \rightarrow 0$. Thus, assuming we have only an upper bound on the satellite velocity, i.e., its velocity may be anywhere in the range of 0–10 km/sec, we choose $\Delta f = f_n \sim 2$ GHz and $B \sim 20$ kHz. The MDP for this system would, therefore, be $\sim (3^{1/2} h\nu/\eta)\ (B f_n)^{1/2}$, which is equivalent to the MDP obtained from a conventional setup with a bandwidth of approximately 10 MHz. If the Doppler shift is more confined, the MDP is correspondingly reduced. For strong returns, of course, the SNR will show an enhancement commensurate with the bandwidth B. Thus, the advantages of the three-frequency heterodyne system may be secured with such a radar. Similar results would be obtained at other frequencies; in the microwave, for example, f_c may be made as small as tens of Hz. In some cases, it may be possible to reduce clutter by the insertion of an extremely sharp notch filter at exactly f_c.

XIII. Application to an Analog Communications System

Use of the three-frequency method for a communications system (in which the transmitter and receiver may be moving relative to each other) is similar to the radar already described, and is indicated in Fig. 13. Note, however, that only one of the carrier waves (f_2) is modulated, and that a demodulator is included. By modulating only one of the beams, the $s \times s$ component reaching the demodulator results from the convolution of a delta function (at f_1) with the modulated signal (centered at f_2), which is simply the original undistorted spectral information ready for demodulation by a suitable device such as a mixer, an envelope detector, or a discriminator. The maximum rate at which modulation may be decoded (or the information capacity) of the system will, of

course, depend on the time response of the system, which is usually governed by the final bandwidth B. We could, in the alternative, construct an analog FM communication system in which a single frequency laser beam is split into two frequencies by a modulator (e.g., an acoustoopitc modulator[12]). In that case, the frequency difference f_c will carry the information. In the absence of information (i.e., f_c constant), f_c will be spectrally very pure (it should be as narrow as the spectral width of the modulator drive signal). Thus the three-frequency nonlinear system could provide the advantage of lower deviation and thereby provide bandwidth compression.

XIV. Summary

The three-frequency nonlinear heterodyne scheme is found, in certain respects, to have advantages over the conventional two-frequency system. One advantage is the possibility of increasing the signal-to-noise ratio and detection sensitivity, particularly when little Doppler information is available. It provides an output signal at a well-known difference frequency regardless of the Doppler shift of the transmitted signals. The usual frequency scanning of the LO or receiver is therefore eliminated. It allows a target to be continuously observed with Doppler shifts of considerably greater magnitude and range than previously possible. The system is also angle independent in the sense that the Doppler shift is proportional to the radial velocity and therefore is generally a function of angle. A wide bandpass filter following the square-law device can be gradually narrowed about $2|f_1' - f_L|$ or $2|f_2' - f_L|$ to obtain Doppler information. If Doppler information is increased, we find that the signal-to-noise ratio can be improved, in accordance with our expectations. The optimum three-frequency nonlinear MDP was obtained assuming full Doppler information was available. Since the use of a two-frequency transmitter can be considered as a special case of a modulated single-frequency beam, the proposed system can be thought of as a heterodyne version of signal extraction at a predetermined modulation frequency. Thus, the technique is similar to heterodyne radiometry[26] but carefully takes into consideration the effects of Doppler shift and signal statistics. Since Doppler shift is generally not an issue in the usual heterodyne radiometer detection scheme, the final filter bandwidth (associated with the integration time) can almost always be made arbitrarily small; furthermore, it is often possible to maintain a fixed phase relationship between the reference and detected signals, so an additional factor of 2 (arising from coherent detection) becomes available. These specific benefits are not available for three-frequency nonlinear heterodyne detection.

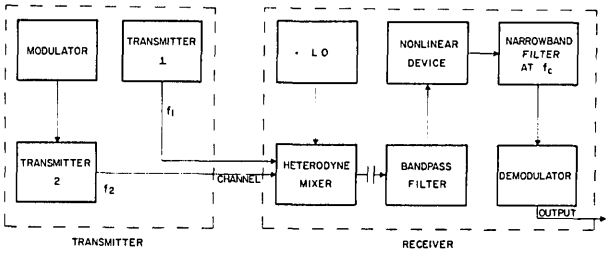

Fig. 13. A three-frequency nonlinear heterodyne analog communications system.

Under the usual conditions of Doppler uncertainty, optimum operation exists with the known difference frequency f_c at a maximum value close to f_n and requires that the radiation power be equally divided between the two received beams. Processing of the dc output from the square-law device was not found to be useful when a blocking capacitor is included in the system. Four-frequency mixing was found to provide acceptable performance only when one of the LO frequencies is substantially attenuated.

Signals of three varieties were considered: (a) sinewave input signals, (b) Gaussian input signals with Gaussian power spectra, and (c) Gaussian input signals with Lorentzian power spectra. Taking the pure sinewave case as a standard, the output signal-to-noise ratio for Gaussian signals is degraded by the factor $[2\Phi(u) - 1] < 1$ (for Gaussian spectra) or by the factor $(1/\pi)\tan^{-1}[4v/(4 - v^2)] < 1$ (for Lorentzian spectra), where u and v are quantities proportional to the bandwidth B of the final narrowband filter. In all cases, decreasing B serves to increase the signal-to-noise ratio and decrease the minimum detectable power. In the Gaussian cases, it was found desirable to keep the width of the spectra as small as possible to maximize the signal-to-noise ratio.

The principle is applicable in all regions of the electromagnetic spectrum where conventional heterodyne detection is useful.

This work was supported in part by the National Science Foundation. One of us (M.C.T.) is grateful to the John Simon Guggenheim Memorial Foundation for assistance.

References

1. M. C. Teich, Appl. Phys. Lett. **15**, 420 (1969).
2. M. C. Teich, R. J. Keyes, and R. H. Kingston, Appl. Phys. Lett. **9**, 357 (1966).
3. M. C. Teich, Proc. IEEE **56**, 37 (1968); reprinted in *Infrared Detectors*, R. D. Hudson, Jr. and J. W. Hudson, Eds. (Dowden, Hutchinson & Ross, Stroudsburg, 1975).
4. M. C. Teich, Proc. IEEE **57**, 786 (1969).
5. M. C. Teich, "Coherent Detection in the Infrared," in *Semiconductors and Semimetals*, R. K. Willardson and A. C. Beer, Eds. (Academic, New York, 1970), Vol. 5, *Infrared Detectors*, ch. 9, p. 361.
6. A. T. Forrester, R. A. Gudmundsen, and P. O. Johnson, Phys. Rev. **99**, 1691 (1955).
7. A. E. Siegman, S. E. Harris, and B. J. McMurtry, "Optical Heterodyning and Optical Demodulation at Microwave Frequencies," in *Optical Masers*, J. Fox, Ed. (Wiley, New York, 1963), pp. 511–527.
8. S. Jacobs and P. Rabinowitz, "Optical Heterodyning with a CW Gaseous Laser," in *Quantum Electronics III*, P. Grivet and N. Bloembergen, Eds. (Columbia U. P., New York, 1964), pp. 481–487.

9. L. Mandel, J. Opt. Soc. Am. **56**, 1200 (1966).
10. S. J. Ippolito, S. Rosenberg, and M. C. Teich, Rev. Sci. Instrum. **41**, 331 (1970).
11. M. C. Teich and R. Y. Yen, J. Appl. Phys. **43**, 2480 (1972).
12. R. L. Abrams and R. C. White, Jr., IEEE J. Quantum Electron. **QE-8**, 13 (1972).
13. M. C. Teich and R. Y. Yen, Appl. Opt. **14**, 680 (1975).
14. W. B. Davenport, Jr. and W. L. Root, *An Introduction to the Theory of Random Signals and Noise* (McGraw-Hill, New York, 1958), p. 112.
15. M. C. Teich, Appl. Phys. Lett. **14**, 201 (1969).
16. M. C. Teich, "Quantum Theory of Heterodyne Detection," in *Proceedings of the Third Photoconductivity Conference,* E. M. Pell, Ed. (Pergamon, New York, 1971), pp. 1–5.
17. D. J. Angelakos and T. E. Everhart, *Microwave Communications* (McGraw-Hill, New York, 1968), p. 204.
18. Ref. 14, pp. 257–259.
19. Ref. 14, p. 255.
20. R. Y. Yen, "Optical Communications: An Investigation of Several Techniques," Ph.D. thesis, Columbia University, 1972.
21. Ref. 14, p. 308.
22. M. I. Skolnik, *Introduction to Radar Systems* (McGraw-Hill, New York, 1958), p. 185.
23. W. E. Murray, Jr., "Coherent Laser Radar Doppler Signatures," in *Optics Research,* MIT Lincoln Lab., 1969, No. 1, p. 6.
24. H. A. Bostick, IEEE. J. Quantum Electron. **QE-3**, 232, (1967).
25. H. A. Bostick and L. J. Sullivan, "Laser Radar and Tracking," in *Optics Research,* MIT Lincoln Lab., 1969, No. 1, p. 21.
26. J. H. McElroy, Appl. Opt. **11**, 1619 (1972).